Nanomorphogenesis of interlayered polyamide membranes for precise ion sieving in lithium extraction

Shi, Yongxuan ; Mai, Zhaohuan ; Guan, Kecheng ; Li, Bowen ; Shen, Qin ; Song, Qiangqiang ; Fu, Wenming ; Xiang, Shang ; Takagi, Ryosuke ;…

(Citation)
Water Research,274:123063

(Issue Date)
2025-04-15

(Resource Type)
journal article

(Version)
Version of Record

Water Research 274 (2025) 123063

Contents lists available at ScienceDirect

Water Research

journal homepage: www.elsevier.com/locate/watres

Nanomorphogenesis of interlayered polyamide membranes for precise ion sieving in lithium extraction

Yongxuan Shi [a,b], Zhaohuan Mai [a,**], Kecheng Guan [a], Bowen Li [a], Qin Shen [a,b], Qiangqiang Song [a,b], Wenming Fu [a,b], Shang Xiang [a,b], Ryosuke Takagi [a], Hideto Matsuyama [a,b,*]

[a] Research Center for Membrane and Film Technology, Kobe University, 1-1 Rokkodaicho, Nada, Kobe 657-8501, Japan
[b] Department of Chemical Science and Engineering, Kobe University, 1-1 Rokkodaicho, Nada, Kobe 657-8501, Japan

ARTICLE INFO

Keywords:
Nanofiltration
Polyamide membrane
Sulfonated carrageenan interlayer
Lithium extraction

ABSTRACT

Nanofiltration (NF) offers a scalable and energy-efficient method for lithium extraction from salt lakes. However, the selective separation of lithium from magnesium, particularly in brines with high magnesium concentrations, remains a significant challenge due to the close similarity in their hydrated ionic radii. The limited Li^+/Mg^{2+}selectivity of current NF membranes is primarily attributed to insufficient control over pore size and surface charge. In this study, we report the development of an interlayered thin-film composite (iTFC) membrane incorporating functionalized sulfonated carrageenan to regulate the interfacial polymerization process. This integrated interlayer plays a crucial role in controlling the diffusion and spatial distribution of amine monomers, leading to the formation of dense, nano-striped polyamide networks. These structural improvements including refined pore size and reduced negative charge significantly enhanced Li^+/Mg^{2+}selectivity (133.5) and increased permeance by 2.5 times compared to conventional TFC membranes. Additionally, the nano-striped structure optimized the membrane filtration area while minimizing ion transport resistance, effectively overcoming the traditional trade-off between ion selectivity and permeability. This study highlights the potential of iTFC membranes for achieving both high lithium purity and recovery, offering a promising avenue for large-scale lithium extraction from brines.

1. Introduction

The rapid expansion of electric mobility and renewable energy technologies has driven a significant increase in global demand of lithium due to its critical role in battery production (Levin et al., 2023; Speirs et al., 2014). Such rising demand promotes the urgent advancement in sustainable and scalable methods for lithium extraction (Roy et al., 2022; Vera et al., 2023). To alleviate the future shortage of lithium, the recovery of lithium from seawater and salt-lake brine has gained prominence over the past few decades (Razmjou et al., 2019; Villalobos et al., 2023; Zhang et al., 2024). However, commercial methods like evaporation and chemical precipitation face challenges, especially when dealing with salt-lakes containing high Mg^{2+}/Li^+ ratios (MLR) (An et al., 2012; Guo et al., 2016; Huang et al., 2021; Tansel, 2012; Xu et al., 2021). Moreover, the conventional evaporation process requires high consumption of freshwater to produce Li_2CO_3, aggravating the water scarcity in arid regions (Foo et al., 2024). Consequently, advancing technologies that can selectively eliminate Mg^{2+} from Mg-rich brines is crucial for ensuring a sustainable Li supply.

Nanofiltration (NF) has emerged as a promising operation for Li/Mg separation, benefiting from high energy efficiency and cost-effectiveness (Fang et al., 2024; Gan et al., 2024; Zhang et al., 2025). On premise of proper membrane properties, a selective NF membrane facilitates the elimination of multivalent cations such as Mg^{2+} and Ca^{2+} from ion mixtures, minimizing the formation of by-product precipitates and improving lithium yield (Sarkar et al., 2021; Zhao et al., 2021). Typically, commercial thin-film composite (TFC) NF membranes feature a polyamide active layer crosslinked via interfacial polymerization between piperazine (PIP) and trimesoyl chloride (TMC), supported by a porous substrate (Mo et al., 2012; Werber et al., 2018). However, conventional negatively charged NF membranes generally exhibit moderate Mg^{2+}rejection due to insufficient size sieving, while the unsatisfactory

* Corresponding author at: Research Center for Membrane and Film Technology, Kobe University, 1-1 Rokkodaicho, Nada, Kobe 657-8501, Japan.
** Corresponding author.
E-mail addresses: zhaohuan.mai@people.kobe-u.ac.jp (Z. Mai), matuyama@kobe-u.ac.jp (H. Matsuyama).

https://doi.org/10.1016/j.watres.2024.123063
Received 22 October 2024; Received in revised form 12 December 2024; Accepted 27 December 2024
Available online 27 December 2024

Li^+permeance is primarily due to strong Donnan exclusion (Aydogan Gokturk et al., 2022; Ritt et al., 2020). Furthermore, current NF membranes are subjected to the inherent trade-off between permeability and selectivity, often necessitating a sacrifice in membrane permeability to ensure sufficient ion selectivity (Geise et al., 2011; Park et al., 2017). As such, an ideal NF membrane for lithium extraction should overcome this trade-off, enabling rapid Li^+ transport while maintaining high Mg^{2+} rejection, hence achieving both high Li purity and Li recovery (Wang et al., 2023).

Previous studies have primarily aimed to achieve both high Li purity and Li recovery mainly based on two strategies: (1) finely tuning the membrane nanopores and (2) finely adjusting the charge of polyamide networks (Dai et al., 2023; Yuan et al., 2020). The Donnan-enhanced strategy takes the advantages of strong electrostatic exclusion to improve the rejection of multivalent cations (e.g., Mg^{2+}) over monovalent cations (e.g., Li^+) (Foo et al., 2023). This strategy typically involves using the monomers or modifiers with cationic moieties like quaternary ammonium (-NR_4^+) groups during interfacial polymerization, where the positive surface charge of polyamide networks can be intensified through 'amine-acyl' or 'hydroxyl-acyl' condensation reactions (Peng and Zhao, 2021; Xu et al., 2022). In many cases, however, the Donnan-enhanced strategy resulted in a loose polyamide structure with larger mean pore diameter than hydration diameter of Mg^{2+}, compromising the size sieving effect and reducing ion selectivity (Chen et al., 2023; Peng et al., 2023c; Wang et al., 2024; Yin et al., 2023). There are few reports on Donnan-enhanced NF membranes with sufficiently high positive surface charge to generate strong electrostatic repulsion, thereby preventing Mg^{2+} permeation (>95 % rejection of $MgCl_2$) (Guo et al., 2024; Li et al., 2024). Overall, the employment of Donnan-enhanced strategy independently to enhance the Mg^{2+} rejection while preserving other critical membrane properties such as pore structure and hydrophilicity still remains a significant challenge (Peng et al., 2023a, 2023b).

Another promising approach involves refining polyamide networks to achieve a more uniform pore structure, which has shown great potential in enhancing Li^+/Mg^{2+} separation efficiency. Main strategies typically include: (1) incorporating additives such as surfactants, nanofillers, macromolecules or salts into the aqueous or organic phase (Liang et al., 2020; Qiu et al., 2021; Shen et al., 2022; Tan et al., 2018), and (2) inducing an interlayer with functional groups like -OH and -COOH between the substrate and the active polyamide layer (Li et al., 2023; Shi et al., 2023; Wang et al., 2018; Yuan et al., 2024; Zhao et al., 2023). These strategies can effectively regulate the distribution and diffusion-reaction dynamics of monomers during interfacial polymerization, finally influencing the pore size uniformity of the resultant polyamide networks. For instance, Peng et al. demonstrated that using a uniformly assembled surfactant monolayer at water/oil interface could facilitate the amine monomer diffusion into organic phase, narrowing the membrane pore size range of 3.2–8.0 Å. This refined pore range enabled an impressive 99.96 % rejection of Mg^{2+} solely based on the size sieving effect, highlighting the importance of controlled and uniform diffusion of amine monomers during interfacial polymerization (Peng et al., 2024). Nevertheless, challenges like the aggregation of additives and uneven distributed interlayer often weaken the regulatory effects on monomer diffusion-reaction behaviors, leading to a wide effective pore size distribution and insufficient ion selectivity for Li^+/Mg^{2+} separation (Zhang et al., 2021). Therefore, developing an effective interlayer strategy to uniformly refine the monomer diffusion behaviors is urgently needed to prepare high-performance NF membranes capable of efficient Li^+/Mg^{2+} separation.

In this study, we developed an interlayered TFC (iTFC) membrane utilizing functional sulfonated carrageenan (CRG). The OSO_3^- groups of CRG played a crucial role in regulating the diffusion of amine monomers during interfacial polymerization process, resulting in a nano-striped polyamide structure. Such crumpled structure provided thinner thickness and increased filtration area, which significantly shortened the water permeation pathway and reduced ion transport resistance, leading to a 2.5-fold increase in permeance compared to traditional TFC membranes with nodular structures. Additionally, the strong interaction between OSO_3^- groups of the interlayer and aqueous amine monomers facilitated the monomer enrichment at the water/oil interface, ensuring uniform monomer distribution and sufficient monomer supply. The uniform monomer diffusion resulted in the formation of a dense polyamide network with narrow pore size distribution and decreased negative charge, exhibiting high Mg^{2+}rejection up to 99.4 %. Moreover, the excellent rejection of Mg^{2+} via size sieving created a concentration gradient of Cl^- across the membrane, promoting Cl^- migration and facilitating the rapid transport of $Li^+$to maintain charge neutrality. Overall, the iTFC membranes effectively overcome the trade-off between ion selectivity and permeability, demonstrating the potential of interlayer-induced interfacial polymerization for efficient lithium extraction from brine and advancing highly efficient ion separation.

2. Experimental section

2.1. Fabrication of TFC and iTFC membranes

The interlayered polyethersulfone (PES) substrates were fabricated via the crosslinking reaction between carrageenan and glutaraldehyde (GA) (Distantina et al., 2013; Nanaki et al., 2015), as detailed in the Supplementary Information. The interlayered substrates were designated as PES-*x*, where *x* correspond to kappa- (*k*-), iota- (*i*-) and lambda- (*λ*-) carrageenan, respectively.

Next, the TFC and iTFC membranes were fabricated by interfacial polymerization on PES and interlayered substrates, respectively. Briefly, the substrates were first immersed in a 3.0 wt% PIP aqueous solution for 2 min, followed by immersion in a 0.10 wt% TMC/*n*-hexane solution for 1 min. After gently rinsing with *n*-hexane, the membrane was placed in an oven at 60 °C for 5 min. The obtained membranes were designated as iTFC-*x* membranes in accordance with the PES-*x* substate. For comparison, a TFC membrane without the interlayer was fabricated on a pristine PES substrate using the same interfacial polymerization procedure.

2.2. Membrane separation performance

The separation performances of the TFC and iTFC NF membranes were evaluated using a lab-scale crossflow setup with an effective area of 7.06 cm^2 (Xu et al., 2024, 2023). The membranes were pre-compacted for 30 min at 5.0 bar to achieve a stable flux and rejection. The permeance (P, $L{\cdot}m^{-2}{\cdot}h^{-1}{\cdot}bar^{-1}$) of each TFC or iTFC membranes was expressed as:

$$P = \frac{\Delta V}{A \times \Delta P \times \Delta t} \quad (1)$$

where ΔV (L) is the permeate volume, A (m^2) is the effective membrane area, ΔP (bar) is the operating pressure, and Δt (h) is the filtrate collection time, respectively.

The concentration of the feed solution (Na_2SO_4, $MgSO_4$, $MgCl_2$, $CaCl_2$, LiCl or NaCl) was 1000 ppm. The salt rejection (R, %) of the NF membranes was calculated by the equation:

$$R = \frac{C_f - C_p}{C_f} \times 100\ \% \quad (2)$$

where C_f and C_p represent the salt concentrations of the feed and permeate solutions, respectively. Salt concentrations were determined from the conductivity measurements (Ultrameter II™ 4P, Myron L Company, Japan).

The Mg^{2+}/Li^+ ratios (10:1, 20:1, 40:1, and 60:1) and total salt concentrations (2000 ppm, 3000 ppm, 4000 ppm, and 5000 ppm) were selected to represent the typical ionic compositions found in natural salt lakes and brine solutions used in lithium extraction processes. The

selective separation factor ($S_{Mg^{2+}/Li^{+}}$) was calculated by the equation:

$$S_{Mg^{2+}/Li^{+}} = \frac{C_f(Mg)/C_f(Li)}{C_P(Mg)/C_P(Li)} \quad (3)$$

where $C_f(Mg)$ and $C_f(Li)$ refer to the concentrations of Li^+ and Mg^{2+} ions in the feed solution, respectively; and $C_P(Mg)$ and $C_P(Li)$ represent the concentrations of Li^+ and Mg^{2+} ions in the permeate solution, respectively. The concentrations of Li^+ and Mg^{2+} in the mixed salt solution were measured using an Inductively Coupled Plasma Optical Emission Spectrometer (ICPOES, Shimadzu, Japan).

2.3. Molecular dynamic (MD) simulations

The diffusive properties of amine monomers in the systems with and without carrageenan interlayers were investigated by MD simulations using the software Materials Studio 2023. Details regarding model construction and simulation parameters are provided in the Supplementary Information.

3. Results and discussion

3.1. Formation of interlayered-PES substrates

To precisely modulate the distribution density of functional groups on the interlayers, three types of carrageenan with varying numbers of OSO_3^- groups were employed to crosslink with GA (Fig. 1**a**). Elemental composition analysis using X-ray photoelectron spectroscopy (XPS) characterizations confirmed the successful incorporation of OSO_3^- groups from the carrageenan interlayer, as evidenced by the higher O/C ratio in the modified substrates compared to the pristine PES membrane (Fig. 1**b**). Previous studies have validated that constructing an interlayer could prevent the formation of defects in polyamide networks and minimize the intrusion of polyamide layer into the large pores of substrate, which are favorable to improve membrane performance (Peng et al., 2020; Shao et al., 2022; Yang et al., 2020). Zeta potential measurements demonstrated that increasing the density of OSO_3^- group density progressively enhanced the negative surface charge, with the PES-λ substrate exhibiting the most negative zeta potential due to its highest OSO_3^- group density (Fig. 1**c**). Water contact angle

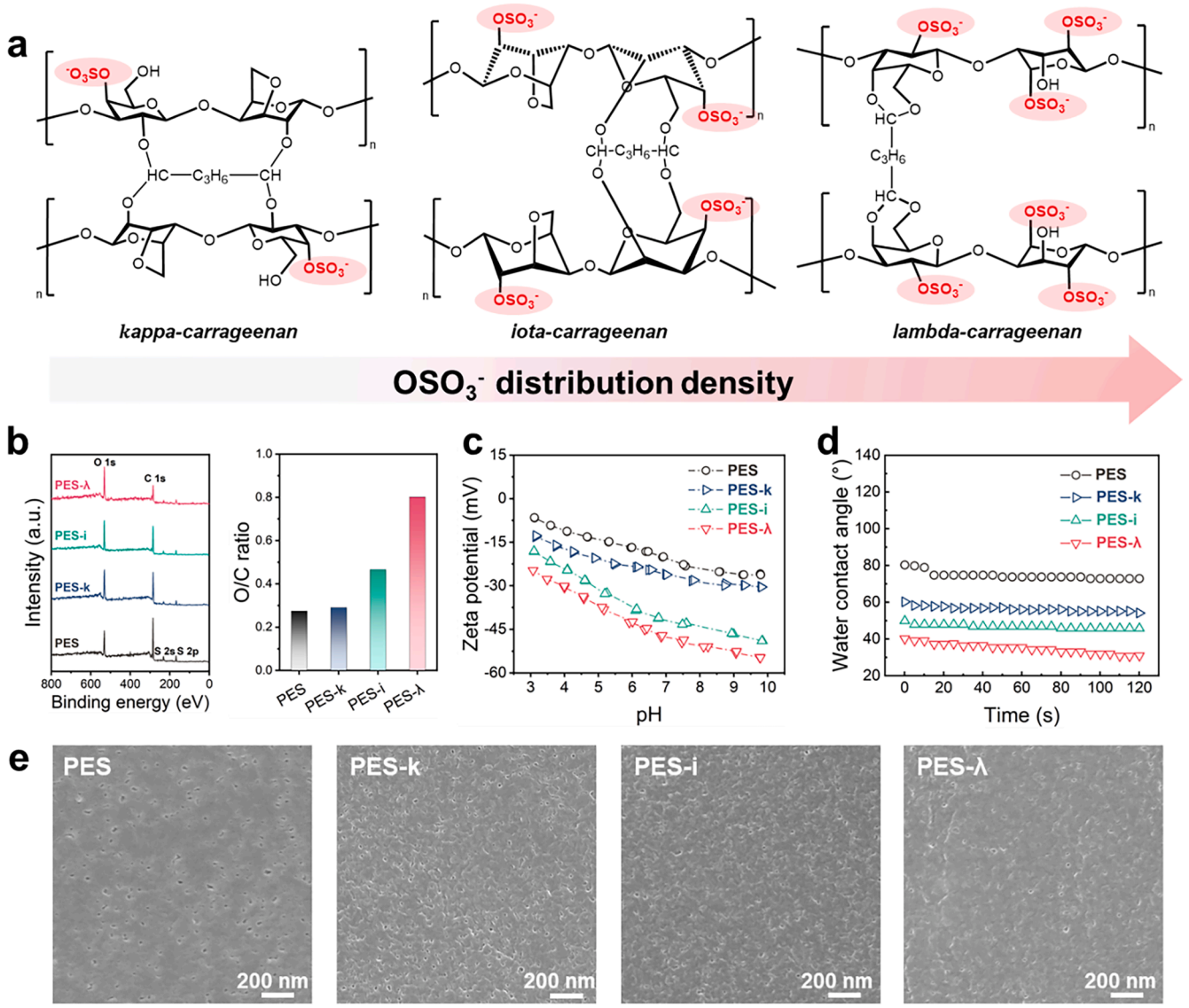

Fig. 1. Characterizations of the pristine and interlayered PES substrates. (a) Schematic illustration of proposed chemical crosslinking reaction between *k*-, *i*-, and λ-carrageenan and GA. Structure properties of the pristine and interlayered PES substrates: (b) X-ray photoelectron spectroscopy profiles and O/C ratios, (c) zeta potentials, (d) water contact angles and (e) surface scanning electron microscopy images.

measurements further showed the improved hydrophilicity consistent with the increased negative charge (Fig. 1**d**). SEM images indicated that the incorporation of porous carrageenan interlayers (PES-*k*, PES-*i* and PES-*λ*) led to a more uniform and reduced pore size in comparison to the pristine PES substrate (Fig. 1**e**). Among the modified substrates, PES-*λ* substrate exhibited the optimal wettability and surface charge, corresponding to the highest density of OSO_3^- groups, which is expected to influence the monomer distribution and diffusion-reaction dynamics during subsequent interfacial polymerization processes.

3.2. Microscopic morphologies of TFC and iTFC membranes

To better understand the impact of the interlayer on polyamide network formation, the scanning electron microscopy (SEM) and atomic force microscopy (AFM) were conducted to analyze the surface morphologies of TFC and iTFC membranes, and field-emission transmission electron microscopy (FETEM) was used to investigate their cross-sectional structures. SEM images revealed the distinctive morphological differences between the iTFC membranes (iTFC-*k*, iTFC-*i* and iTFC-*λ*) and TFC membrane (Fig. 2**a**). The TFC membrane featured a typical nodular structure with uniform surface morphology (Song et al., 2021), whereas the iTFC membranes displayed rougher surfaces with densely packed nano-striped polyamide networks. AFM measurements further confirmed that the iTFC-*λ* membrane exhibited the most refined and uniform nano-striped structure among the three iTFC membranes, with higher surface roughness compared to iTFC-*k* and iTFC-*i* (Fig. 2b and c). These morphological differences might be attributed to the increased density of OSO_3^- groups on PES-*λ* interlayer, which enables more precise control over the initial distribution and subsequent diffusion of amine monomers during the interfacial polymerization process. In contrast, the iTFC-*k* membrane with fewer OSO_3^- groups displayed fewer and less defined stripe patterns within the polyamide structure. Cross-sectional TEM analysis revealed that the iTFC membranes with nano-striped polyamide nanofilms were significantly thinner (~35 nm) compared to the TFC membranes (~94 nm) (Fig. 2**d**). The reduced thickness of the polyamide layer would lower the water resistance to transport across the active layer (Hu et al., 2023). Moreover, the uniform and interconnected nanovoids inside the polyamide networks can greatly shorten the water pathway distance. Overall, these findings demonstrated the critical role of the interlayer in modulating interfacial polymerization process, leading to distinct morphological differences in polyamide networks, which are expected to further influence membrane properties and final separation performance.

3.3. Mechanistic insights into the nanomorphogenesis of the iTFC membranes

Our previous studies have highlighted the importance of the striped polyamide regularity and aspect ratio (i.e., height/lateral dimension) in optimizing membrane performance (Shi et al., 2024). In the current

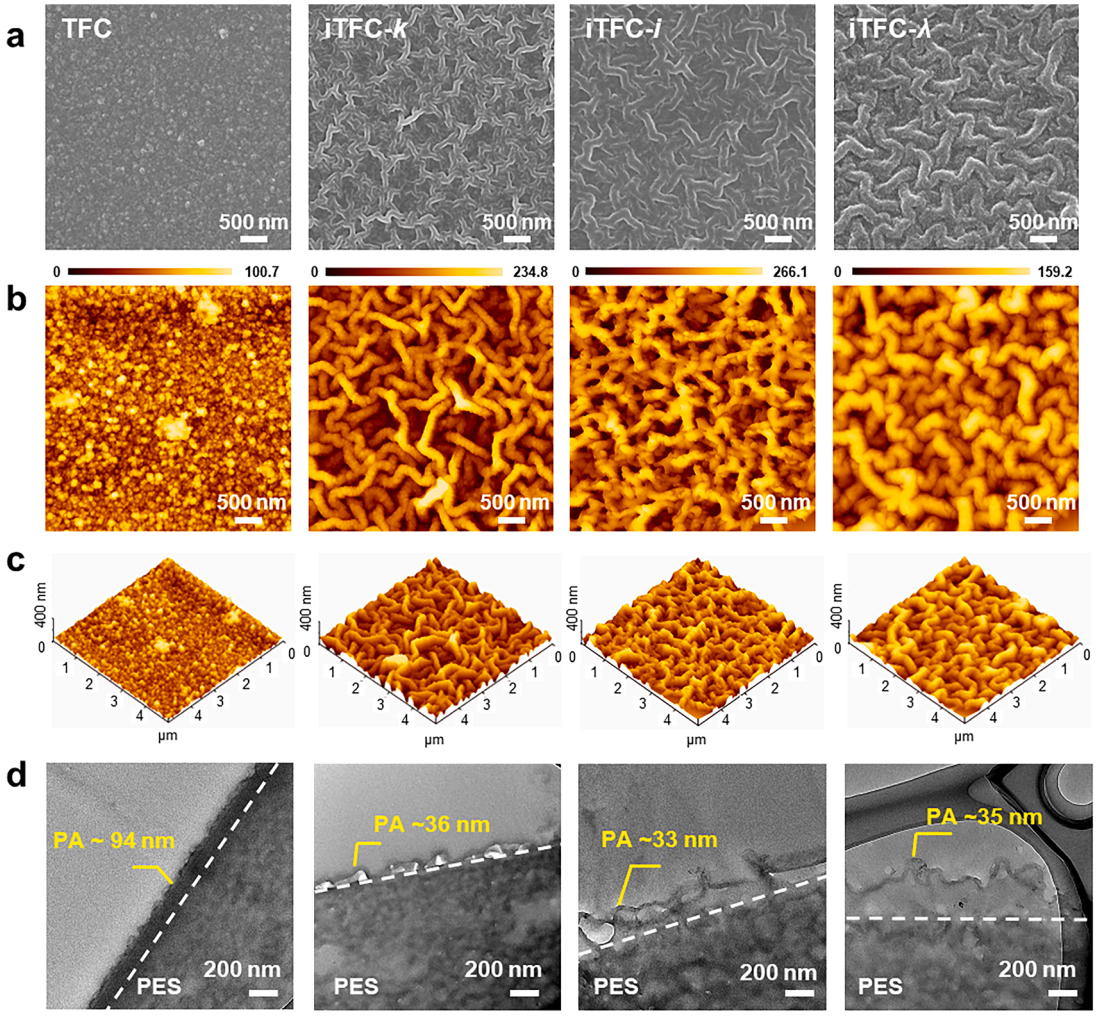

Fig. 2. Morphological characterizations of TFC and iTFC membranes: (a) SEM images, (b) AFM view of top surface (c) tapping mode AFM topographic images and (d) cross-section TEM images.

work, variations in the morphological features such as the width and aspect ratio of the polyamide networks were observed among the iTFC membranes. We suppose this may be attributed to the distribution density of functional groups which affect the initial monomer distribution and the subsequent diffusion rate of amine monomers. To clarify our assumption, MD simulations were conducted to better understand the roles of interlayers during the formation of polyamide nanofilms (Fig. 3**a–d**). The diffusive behavior of PIP monomers was analyzed in models with and without the interlayer by evaluating their mean square displacement (*MSD*). The dynamic movement of PIP can be inferred from the slope derived from linear regression between the *MSD* and simulation time. The results indicated a significant decrease in PIP diffusion coefficient from 6.0×10^{-9} $m^2 \cdot s^{-1}$ to 1.3×10^{-9} $m^2 \cdot s^{-1}$ in the presence of interlayer due to the interaction between the functional groups (i.e., OSO_3^- and -OH) and PIP monomers *via* electrostatic interaction and hydrogen bonding (Fig. 3**e and Fig. S1)**. Numerous studies have demonstrated the retarded effect on PIP diffusion could impose an impact on polyamide growth during interfacial polymerization (Shen et al., 2023; Song et al., 2022). In the interlayer-containing systems, sufficiently large diffusivity difference between TMC (approximately

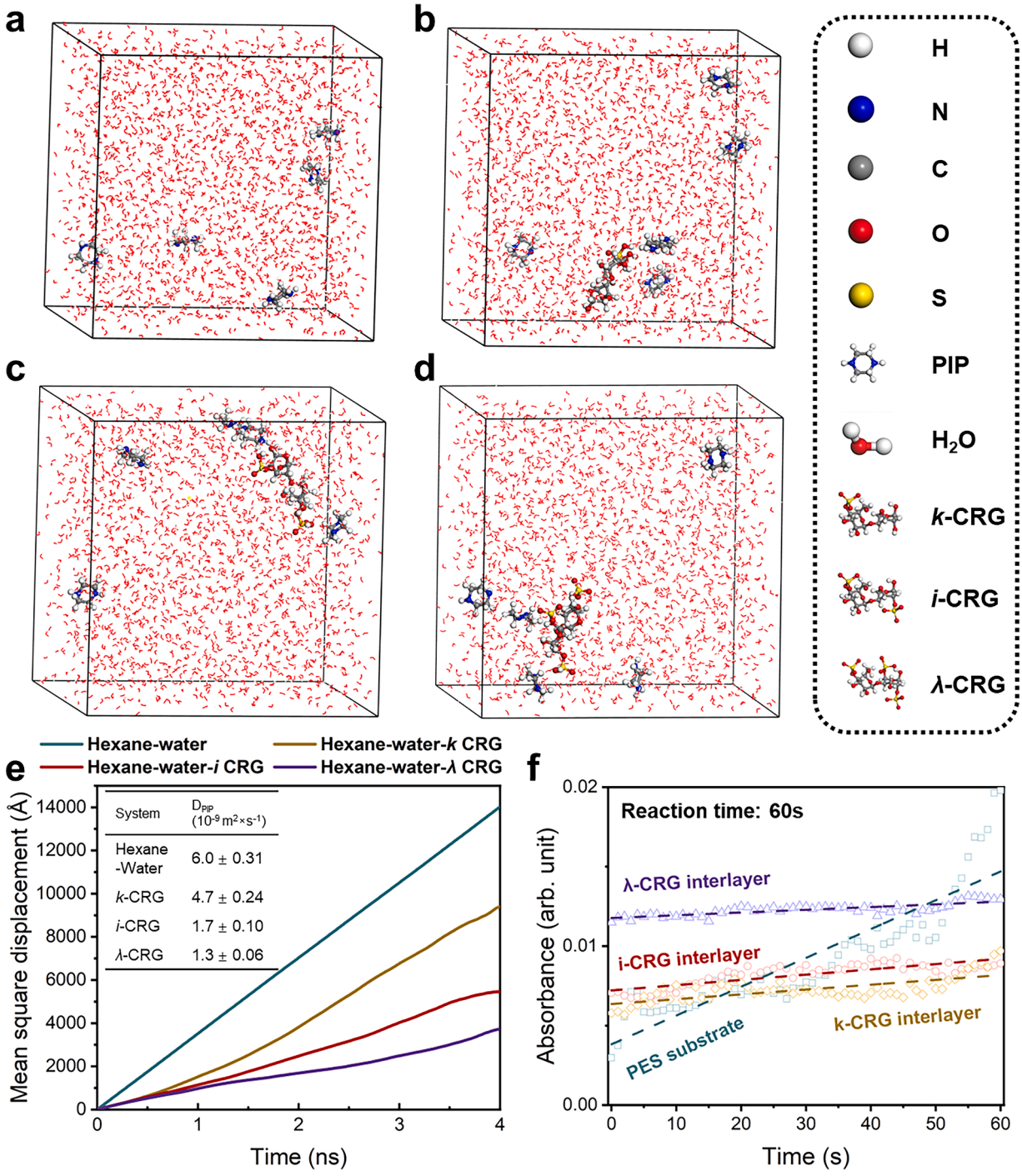

Fig. 3. Mechanistic insights into the nanomorphogenesis of the iTFC membranes. (a) Snapshot of PIP in pure water system, (b) *k*-CRG–water system, (c) *i*-CRG–water system and (d) *λ*-CRG–water system during MD simulations. (e) Diffusive properties of PIP and (f) UV–vis spectra of PIP in organic phase for interlayer-free and interlayer-contained systems.

10^{-9} $m^2 \cdot s^{-1}$) and PIP (10^{-10} $m^2 \cdot s^{-1}$) was met (Tan et al., 2018), facilitating the formation of Turing-patterns on the polyamide nanofilms. In contrast, the smoother nodular patterns were exhibited on traditional polyamide nanofilms without sufficient diffusivity difference.

Beyond the retarded diffusion dynamics of PIP monomers, their initial distribution and local concentration at the water/*n*-hexane interface also determine the properties of the polyamide networks formed during interfacial polymerization. Ultraviolet-visible (UV–vis) spectroscopy measurements were conducted to quantify the amounts PIP diffusing into the organic phase across various substrates (Fig. 3f). The linear regression slopes between PIP absorbance and diffusion time for the four systems (i.e., PES substrate, and *k*-, *i*-, and *λ*-interlayered substrates) indicated restricted PIP diffusion in all three interlayered systems, aligning with the MD simulation results. Additionally, the initial concentration of PIP in the organic phase was significantly higher on the interlayered substrates compared to the pristine PES substrate.

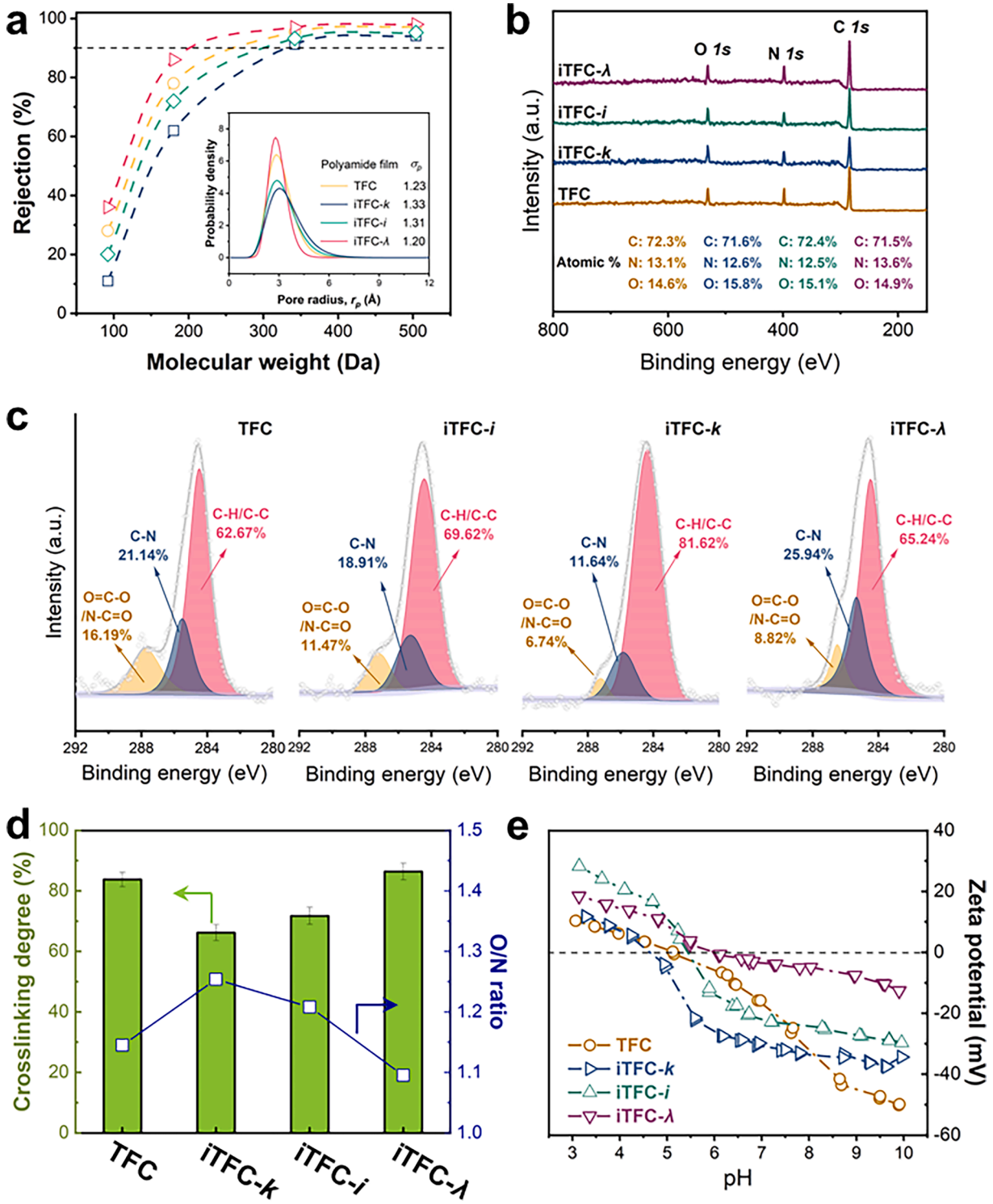

Fig. 4. Physicochemical properties of TFC and iTFC membranes. (a) MWCO and pore size distribution, (b) XPS profiles, (c) the high-resolution of C 1s spectra, (d) crosslinking degree calculated based on O/N ratio from XPS profiles, and (e) zeta potentials.

This can be attributed to the enrichment effect of the interlayers, where strong electrostatic interactions between the negatively charged OSO_3^- groups and the amine monomers promote PIP accumulation at the reaction interface.

The enrichment and controlled diffusion of PIP at the interface are critical elements of nanomorphogenesis, the self-organized evolution of nanoscale features during interfacial polymerization. As demonstrated by UV–vis data, the amount of PIP diffused through the interlayered substrates increased with the OSO_3^- group density, leading to enhanced monomer accumulation at the reaction interface. The higher OSO_3^- group density on the interlayer facilitated a more uniform initial distribution of PIP at the reaction interface, leading to the formation of polyamide networks with well-ordered nano-striped structures and increased characteristic heights. These results align with the observed morphological trends across the PES-λ substrates, showing that variations in OSO_3^- group density or PIP concentrations had consistent effects on the polyamide morphology. Increasing PIP concentration resulted in higher local monomer density at the reaction interface, accelerating polymerization and producing more pronounced crumpled structures (**Fig. S2 and Fig. S3**). Similarly, higher CRG concentrations introduced more OSO_3^- groups, strengthening interactions with PIP monomers and contributing to enhanced nano-structuring of the polyamide layer (**Fig. S4 and Fig. S5**). Despite these variations, the nanomorphogenesis process ensured that both PIP and OSO_3^- group density consistently promoted the formation of uniform and dense polyamide networks, resulting in stable ion separation performance. In summary, the interlayer played a dual role in enriching PIP monomers at the reaction interface and regulating their diffusion, thereby facilitating the self-organization of structured polyamide networks with nano-striped morphology, which was expected to further improve the membrane separation performance.

3.4. Characterizations of TFC and iTFC membranes

The pore size of TFC and iTFC membranes was determined based on the rejections of neutral molecules with different molecular weights (Fig. 4**a**). The results indicated that iTFC-*k* membrane exhibited a larger molecular weight cut-off (MWCO) value and wider pore size distribution than those of TFC membrane. This broader distribution can be attributed to the looser polyamide network structure in the iTFC-*k* membrane. The lower density of OSO_3^- groups diminished the enrichment effect on PIP monomers via electrostatic attraction, leading to an inadequate accumulation of PIP monomers at the reaction interface. Consequently, the resulting polyamide network for iTFC-*k* membrane exhibited inhomogeneous pores with a lower crosslinking degree, as confirmed by XPS analysis (Fig. 4**b–d**). In contrast, the regulatory effect on amine monomer diffusion and distribution was effectively improved as the OSO_3^- distribution density increased, ensuring controlled and consistent monomers supply during interfacial polymerization. As a result, iTFC-λ membranes exhibited the smaller MWCO value and narrower pore size distribution, indicating the formation of denser polyamide networks with pores that were more homogeneous. Additionally, the sufficient monomer supply led to a more complete interfacial polymerization reaction with fewer residual unreacted groups on the polyamide networks, thus a less negatively charged surface for iTFC-λ membrane (Fig. 4**e**) (Liu et al., 2023). Overall, the optimal iTFC-λ membrane with refined pore size and less negatively charge demonstrated the excellent potential for Li^+/Mg^{2+} separation through size sieving and reduced electrostatic interactions with divalent ions.

3.5. Separation performance

We further investigated the desalination performance of single salts for TFC and iTFC membranes. The iTFC-*k* membrane exhibited a 5-fold increase in permeance, rising from 4.2 $L{\cdot}m^{-2}{\cdot}h^{-1}{\cdot}bar^{-1}$ for TFC membrane to 22.8 $L{\cdot}m^{-2}{\cdot}h^{-1}{\cdot}bar^{-1}$, but accompanied by a decrease in the rejection of $MgSO_4$ (Fig. 5**a**). This significant increase in permeance can be attributed to the crumpled polyamide structure with thinner thickness, which significantly decreased water resistance. While the limited regulatory effect of low distribution density of OSO_3^- groups led to the inhomogeneous interfacial polymerization reaction with insufficient PIP supply, compromising the salt rejection. Elevating the OSO_3^- groups density in the interlayers efficiently improved the even amine monomer distribution and sufficient monomer supply (**Fig. S6** and **Fig. S7**), facilitating a consistent and homogeneous interfacial polymerization reaction, which lead to the formation of a highly cross-linked polyamide structure with a narrow pore size distribution in the iTFC-λ membrane. As a result, the iTFC-λ membrane demonstrated superior Mg^{2+} rejection while achieving twice the water permeance of the TFC membrane (Fig. 5**b and Fig. S8**). The Li^+/Mg^{2+} separation selectivity and water permeance of iTFC-λ membrane were further compared with previously reported membranes, including commercial, polyethylenimine (PEI)-based, PIP-based, layer-by-layer NF membranes. Typically, PEI-based membrane demonstrated high ion selectivity but low permeance, whereas PIP-based membrane showed high permeance with insufficient ion selectivity. In comparison, the iTFC-λ membrane exhibited both enhanced selectivity and permeance, indicating their potential to overcome the trade-off between membrane permeance and selectivity (Fig. 5**c**).

Considering the diverse ionic composition in the natural salt lakes, we further assessed the Li^+/Mg^{2+} separation performance of iTFC-λ membrane under a series of binary $LiCl/MgCl_2$ salt mixtures with different MLR and total salt concentrations as simulated brine solutions (Fig. 5**d** and Fig. 5**e**). As the MLR increased from 10:1 to 60:1 at a total salt concentration of 2000 ppm, the membrane consistently maintained a high rejection of Mg^{2+} (~99 %), while the rejection of Li^+slightly decreased. This effect can be explained that the higher concentration of Mg^{2+} created a competitive environment where Mg^{2+}dominated the interaction with membrane. Additionally, the uniform pore size and reduced negative surface charge enabled iTFC-λ membrane to exhibit a satisfactory level of Mg^{2+} rejection through size sieving and reduced electrostatic attraction toward divalent ions. In turn, the saturation effect caused the increased permeation of Li^+ions with smaller hydrated radius (3.82 Å) and lower charge density, resulting in a decrease in Li^+ rejection as the Mg^{2+}/Li^+ ratio increases. Compared to the traditional TFC NF membranes, iTFC-λ membrane showed both higher permeance and larger rejection difference between Li^+ and Mg^{2+}, consistent with the single salt tests. We further investigated the membrane separation performance with varying salt concentration ranging from 2000 ppm to 5000 ppm while maintaining MLR of 20:1. Even under high salinity solutions, iTFC-λ membrane exhibited a slight decrease in rejection of Mg^{2+}, accompanied by a notable negative rejection of Li^+ up to −17 %. Moreover, the iTFC-λ membrane demonstrated consistent separation performance over a 7-day operation, confirming its stability and durability in separating Li^+/Mg^{2+}(Fig. 5**f**). The observed negative rejection of Li^+ arises from the differential steric resistance experienced by Mg^{2+} and Li^+, as well as the necessity to maintain charge neutrality in the permeate. Since the iTFC membrane exhibited greater steric hindrance toward Mg^{2+}, it led to the accumulation of Mg^{2+} at the feed side, which further resulted in a concentration gradient of Cl^- ions across the membrane. This gradient could drive the transport of Cl^- ions into the permeate side. To maintain zero net electric current in the permeate, a counter-ion must accompany the transported Cl^- ions. Given its lower steric hindrance compared to Mg^{2+}, Li^+ preferentially migrates into the permeate, leading to a higher Li^+ concentration in the permeate relative to the feed and resulting in the observed negative rejection phenomenon (Fig. 5**g**).

Moreover, we applied the SDEM model to determine ion permeability from experimental data to evaluate Li^+ purity and recovery, which are two critical criteria in practical applications. Li^+ purity was assessed by the ratio of Li^+ permeability to Mg^{2+}permeability, while Li^+recovery was evaluated based on the ratio of Li^+ permeability to water permeability. Performance comparisons result further indicated

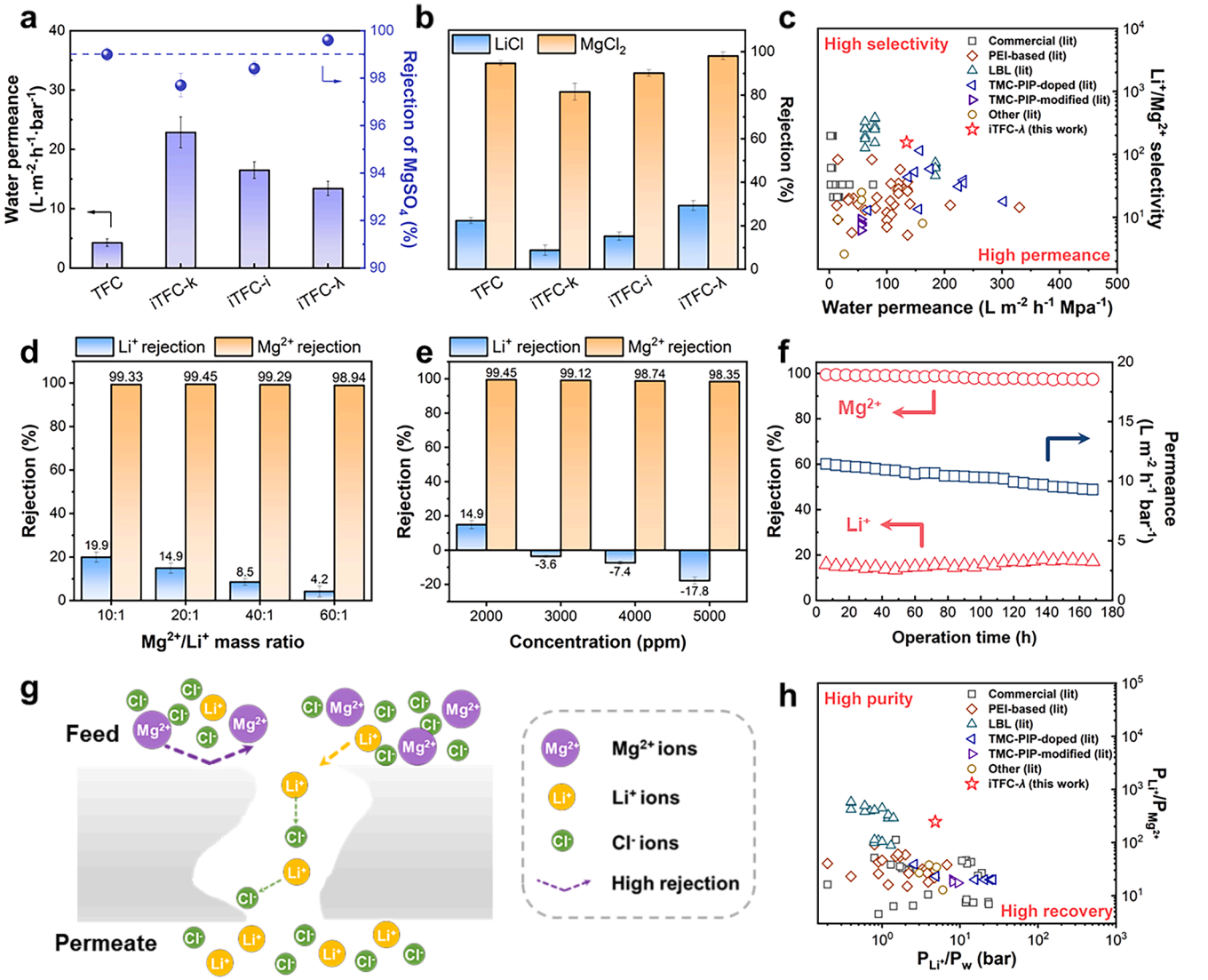

Fig. 5. Li^+/Mg^{2+} separation performances of the TFC and iTFC membranes. (a) Pure water permeance and salt rejection of $MgSO_4$. (b) Salt rejection rates of $MgCl_2$ and LiCl. Each rejection rate was measures using feed solution containing single salt with 1000 ppm. (c) Ion separation performance in terms of Li^+/Mg^{2+} selectivity and water permeance of the iTFC-λ membrane (red) compared with reported NF membranes (**Table S1**). (d) Rejection of Mg^{2+} and Li^+ as a function of MLR. The concentration of the feed solution is maintained at 2000 ppm. (e) Rejection of Mg^{2+} and Li^+ as a function of the salt concentration in the feed solution, with a fixed Mg^{2+}/Li^+ mass ratio of 20:1. (f) Long term stability of iTFC-λ membrane. (g) Schematic of negative rejection during ion separation. (h) Ratio between Li^+ permeability and Mg^{2+} permeability (P^+_{Li}/P^{2+}_{Mg}) versus ratio between Li^+ permeability and water permeability (P^+_{Li}/P_w). An increase in P^+_{Li}/P_w enhances lithium recovery by favoring Li^+ transport over water, while an increase in P^+_{Li}/P^{2+}_{Mg} improves lithium purity by selectively allowing more Li^+ transport relative to Mg^{2+}. The permeability values were calculated using the solution-diffusion-electromigration (SDEM) model, with an assumed mass transfer coefficient of 100 L m^{-2} h^{-1} for both LiCl and $MgCl_2$ solutions (**Table S2**).

the successful achievement in both high Li^+ recovery and purity (Fig. 5**h**). Overall, designing the NF membranes with a uniform and effective pore range smaller than Mg^{2+} radius is crucial for ensuring Li^+ purity. At the same time, precise Mg^{2+} rejection establishes a Cl^- concentration gradient, driving Li^+ co-transport to maintain charge neutrality, finally contributing to the improved Li^+recovery. These findings indicated the potential of negatively-charged iTFC membranes with optimized pore sizes for practical applications.

4. Conclusion

This study demonstrated the successful development of interlayered iTFC NF membranes with optimized microstructures to enhance Li^+/Mg^{2+} separation performance. The incorporation of functional sulfonated carrageenan as an interlayer facilitated the fine control of amine monomer distribution and diffusion during interfacial polymerization, leading to the formation of nano-striped polyamide networks. The structural improvements including smaller pore size, reduced thickness and increased permeable sites effectively improved Mg^{2+} rejection and increased permeance, hence achieving efficient lithium extraction from brine. The findings highlight the importance of interlayer-induced NF membranes in balancing lithium purity and lithium recovery, overcoming the traditional trade-off effects. Future research should focus on further optimizing interlayer composition and monomer distribution to advance NF membrane performance in various ion separation applications.

Declaration of competing interest

The authors declare that they have no known competing financial interests or personal relationships that could have appeared to influence the work reported in this paper.

Acknowledgment

Yongxuan Shi appreciates the financial support from JST SPRING (Grant No. JPMJSP2148).

Supplementary materials

Supplementary material associated with this article can be found, in the online version, at doi:10.1016/j.watres.2024.123063.

References

An, J.W., Kang, D.J., Tran, K.T., Kim, M.J., Lim, T., Tran, T., 2012. Recovery of lithium from Uyuni salar brine. Hydrometallurgy 117-118, 64–70.
Aydogan Gokturk, P., Sujanani, R., Qian, J., Wang, Y., Katz, L.E., Freeman, B.D., Crumlin, E.J, 2022. The Donnan potential revealed. Nat. Commun. 13 (1), 5880.
Chen, K., Li, F., Wei, T., Zhou, H., Zhang, T., Zhao, S., Xie, T., Sun, H., Li, P., Niu, Q.J., 2023. An interlayer-based positive charge compensation strategy for the preparation of highly selective Mg2+/Li+ separation nanofiltration membranes. J. Membr. Sci. 684, 121882.
Dai, R., Zhou, H., Wang, T., Qiu, Z., Long, L., Lin, S., Tang, C.Y., Wang, Z., 2023. Nanovehicle-assisted monomer shuttling enables highly permeable and selective nanofiltration membranes for water purification. Nat. Water 1 (3), 281–290.
Distantina, S., Rochmadi, R., Fahrurrozi, M., Wiratni, W., 2013. Preparation and characterization of glutaraldehyde-crosslinked kappa carrageenan hydrogel. Eng. J. 17 (3), 57–66.
Fang, S., Guan, K., Zhou, S., Song, Q., Shi, Y., Fu, W., Li, Z., Xu, P., Hu, M., Mai, Z., Zhang, P., Matsuyama, H., 2024. Ternary-coordination-regulated polyamide nanofiltration membranes for Li+/Mg2+ separation. Desalination 581, 117577.
Foo, Z.H., Liu, S., Kanias, L., Lee, T.R., Heath, S.M., Tomi, Y., Miyabe, T., Keten, S., Lueptow, R.M., Lienhard, J.H., 2024. Positively-coated nanofiltration membranes for lithium recovery from battery leachates and salt-lakes: ion transport fundamentals and module performance. Adv. Funct. Mater. 34 (48), 2408685.
Foo, Z.H., Rehman, D., Bouma, A.T., Monsalvo, S., Lienhard, J.H., 2023. Lithium concentration from salt-lake brine by donnan-enhanced nanofiltration. Environ. Sci. Technol. 57 (15), 6320–6330.
Gan, N., Lin, Y., Zhang, Y., Qiu, Y., Yu, J., She, Q., Ooya, T., Lin, Q., Matsuyama, H., 2024. Ion-selective supramolecular membrane with pH-regulated smart nanochannels for lithium extraction. J. Membr. Sci. 708, 123035.
Geise, G.M., Park, H.B., Sagle, A.C., Freeman, B.D., McGrath, J.E., 2011. Water permeability and water/salt selectivity tradeoff in polymers for desalination. J. Membr. Sci. 369 (1), 130–138.
Guo, B.-B., Liu, C., Zhu, C.-Y., Xin, J.-H., Zhang, C., Yang, H.-C., Xu, Z.-K., 2024. Double charge flips of polyamide membrane by ionic liquid-decoupled bulk and interfacial diffusion for on-demand nanofiltration. Nat. Commun. 15 (1), 2282.
Guo, Y., Ying, Y., Mao, Y., Peng, X., Chen, B., 2016. Polystyrene sulfonate threaded through a metal–organic framework membrane for fast and selective lithium-ion separation. Angew. Chem. Int. Ed. 55 (48), 15120–15124.
Hu, Y., Wang, F., Yang, Z., Tang, C.Y., 2023. Modeling nanovoid-enhanced water permeance of thin film composite membranes. J. Membr. Sci. 675, 121555.
Huang, T.-Y., Pérez-Cardona, J.R., Zhao, F., Sutherland, J.W., Paranthaman, M.P., 2021. Life cycle assessment and techno-economic assessment of lithium recovery from geothermal brine. ACS Sustain. Chem. Eng. 9 (19), 6551–6560.
Levin, T., Bistline, J., Sioshansi, R., Cole, W.J., Kwon, J., Burger, S.P., Crabtree, G.W., Jenkins, J.D., O'Neil, R., Korpås, M., Wogrin, S., Hobbs, B.F., Rosner, R., Srinivasan, V., Botterud, A., 2023. Energy storage solutions to decarbonize electricity through enhanced capacity expansion modelling. Nat. Energy 8 (11), 1199–1208.
Li, J., Peng, H., Liu, K., Zhao, Q., 2024. Polyester nanofiltration membranes for efficient cations separation. Adv. Mater. 36 (9), 2309406.
Li, Z., Xu, Y., Shen, L., Li, R., Jiao, Y., Lin, H., Tang, C.Y., 2023. Nano-wrinkled polyamide membrane preparation via heterogeneous surface-regulated interfacial polymerization for enhanced desalination performance. Desalination 564, 116801.
Liang, Y., Zhu, Y., Liu, C., Lee, K.-R., Hung, W.-S., Wang, Z., Li, Y., Elimelech, M., Jin, J., Lin, S., 2020. Polyamide nanofiltration membrane with highly uniform sub-nanometre pores for sub-1 Å precision separation. Nat. Commun. 11 (1), 2015.
Liu, W., Long, L., Yang, Z., Wang, L., Gan, Q., Zhou, S., Sarkar, P., Guo, H., Tang, C.Y., 2023. Enhancing the removal of organic micropollutants by nanofiltration membrane with Fe (III)–tannic acid interlayer: mechanisms and environmental implications. Water Res. 245, 120623.
Mo, Y., Tiraferri, A., Yip, N.Y., Adout, A., Huang, X., Elimelech, M., 2012. Improved antifouling properties of polyamide nanofiltration membranes by reducing the density of surface carboxyl groups. Environ. Sci. Technol. 46 (24), 13253–13261.
Nanaki, S.G., Kyzas, G.Z., Tzereme, A., Papageorgiou, M., Kostoglou, M., Bikiaris, D.N., Lambropoulou, D.A., 2015. Synthesis and characterization of modified carrageenan microparticles for the removal of pharmaceuticals from aqueous solutions. Colloids Surf. B: Biointerfaces 127, 256–265.
Park, H.B., Kamcev, J., Robeson, L.M., Elimelech, M., Freeman, B.D., 2017. Maximizing the right stuff: the trade-off between membrane permeability and selectivity. Science (1979) 356 (6343), eaab0530.
Peng, H., Liu, X., Su, Y., Li, J., Zhao, Q., 2023a. Advanced lithium extraction membranes derived from tagged-modification of polyamide networks. Angew. Chem. Int. Ed. 62 (48), e202312795.
Peng, H., Su, Y., Liu, X., Li, J., Zhao, Q., 2023b. Designing gemini-electrolytes for scalable Mg2+/Li+ separation membranes and modules. Adv. Funct. Mater. 33 (51), 2305815.
Peng, H., Yu, K., Liu, X., Li, J., Hu, X., Zhao, Q., 2023c. Quaternization-spiro design of chlorine-resistant and high-permeance lithium separation membranes. Nat. Commun. 14 (1), 5483.
Peng, H., Zhao, Q., 2021. A nano-heterogeneous membrane for efficient separation of lithium from high magnesium/lithium ratio brine. Adv. Funct. Mater. 31 (14), 2009430.
Peng, L.E., Yao, Z., Yang, Z., Guo, H., Tang, C.Y., 2020. Dissecting the role of substrate on the morphology and separation properties of thin film composite polyamide membranes: seeing is believing. Environ. Sci. Technol. 54 (11), 6978–6986.
Peng, Q., Wang, R., Zhao, Z., Lin, S., Liu, Y., Dong, D., Wang, Z., He, Y., Zhu, Y., Jin, J., Jiang, L., 2024. Extreme Li-Mg selectivity via precise ion size differentiation of polyamide membrane. Nat. Commun. 15 (1), 2505.
Qiu, Z.-L., Fang, L.-F., Shen, Y.-J., Yu, W.-H., Zhu, B.-K., Hélix-Nielsen, C., Zhang, W., 2021. Ionic dendrimer based polyamide membranes for ion separation. ACS Nano 15 (4), 7522–7535.
Razmjou, A., Asadnia, M., Hosseini, E., Habibnejad Korayem, A., Chen, V., 2019. Design principles of ion selective nanostructured membranes for the extraction of lithium ions. Nat. Commun. 10 (1), 5793.
Ritt, C.L., Werber, J.R., Wang, M., Yang, Z., Zhao, Y., Kulik, H.J., Elimelech, M., 2020. Ionization behavior of nanoporous polyamide membranes. In: , 117, pp. 30191–30200.
Roy, J.J., Rarotra, S., Krikstolaityte, V., Zhuoran, K.W., Cindy, Y.D.-I., Tan, X.Y., Carboni, M., Meyer, D., Yan, Q., Srinivasan, M., 2022. Green recycling methods to treat lithium-ion batteries e-waste: a circular approach to sustainability. Adv. Mater. 34 (25), 2103346.
Sarkar, P., Modak, S., Karan, S., 2021. Ultraselective and highly permeable polyamide nanofilms for ionic and molecular nanofiltration. Adv. Funct. Mater. 31 (3), 2007054.
Shao, S., Zeng, F., Long, L., Zhu, X., Peng, L.E., Wang, F., Yang, Z., Tang, C.Y., 2022. Nanofiltration membranes with crumpled polyamide films: a critical review on mechanisms, performances, and environmental applications. Environ. Sci. Technol. 56 (18), 12811–12827.
Shen, L., Cheng, R., Yi, M., Hung, W.-S., Japip, S., Tian, L., Zhang, X., Jiang, S., Li, S., Wang, Y., 2022. Polyamide-based membranes with structural homogeneity for ultrafast molecular sieving. Nat. Commun. 13 (1), 500.
Shen, Q., Song, Q., Mai, Z., Lee, K.-R., Yoshioka, T., Guan, K., Gonzales, R.R., Matsuyama, H., 2023. When self-assembly meets interfacial polymerization. Sci. Adv. 9 (18), eadf6122.
Shi, Y., Mai, Z., Shen, Q., Song, Q., Fu, W., Xiang, S., Hu, M., Guan, K., Takagi, R., Matsuyama, H., 2024. Nanomorphogenesis of polyamide membranes by regulating activator-inhibitor diffusivity difference. J. Membr. Sci. 702, 122804.
Shi, Y., Wang, Z., Mai, Z., Shen, Q., Song, Q., Fu, W., Xiang, S., Fang, S., Zhang, P., Chiao, Y.-H., Guan, K., Matsuyama, H., 2023. Nanomorphogenesis of template-induced crumpled polyamide nanofiltration membranes. J. Membr. Sci. 686, 121997.
Song, Q., Lin, Y., Ueda, T., Istirokhatun, T., Shen, Q., Guan, K., Yoshioka, T., Matsuyama, H., 2021. Mechanism insights into the role of the support mineralization layer toward ultrathin polyamide nanofilms for ultrafast molecular separation. J. Mater. Chem. A 9 (46), 26159–26171.
Song, Q., Lin, Y., Ueda, T., Shen, Q., Lee, K.-R., Yoshioka, T., Matsuyama, H., 2022. A zwitterionic copolymer-interlayered ultrathin nanofilm with ridge-shaped structure for ultrapermeable nanofiltration. J. Membr. Sci. 657, 120679.
Speirs, J., Contestabile, M., Houari, Y., Gross, R., 2014. The future of lithium availability for electric vehicle batteries. Renew. Sustain. Energy Rev. 35, 183–193.
Tan, Z., Chen, S., Peng, X., Zhang, L., Gao, C., 2018. Polyamide membranes with nanoscale Turing structures for water purification. Science (1979) 360 (6388), 518–521.
Tansel, B., 2012. Significance of thermodynamic and physical characteristics on permeation of ions during membrane separation: hydrated radius, hydration free energy and viscous effects. Sep. Purif. Technol. 86, 119–126.
Vera, M.L., Torres, W.R., Galli, C.I., Chagnes, A., Flexer, V., 2023. Environmental impact of direct lithium extraction from brines. Nat. Rev. Earth Environ. 4 (3), 149–165.
Villalobos, L.F., Zhang, J., Elimelech, M., 2023. Nanofiltration for circularity: fit-for-purpose design and evaluation. One Earth. 6 (7), 767–771.
Wang, J., Zhang, H., Tian, R., Shen, H., Li, W.-H., Wang, Y., 2024. Enhancing Mg2+/Li+ separation performance of nanofiltration membranes through polyelectrolyte modulation and surface modification. J. Membr. Sci. 701, 122725.
Wang, R., Alghanayem, R., Lin, S., 2023. Multipass nanofiltration for lithium separation with high selectivity and recovery. Environ. Sci. Technol. 57 (38), 14464–14471.
Wang, Z., Wang, Z., Lin, S., Jin, H., Gao, S., Zhu, Y., Jin, J., 2018. Nanoparticle-templated nanofiltration membranes for ultrahigh performance desalination. Nat. Commun. 9 (1), 2004.
Werber, J.R., Porter, C.J., Elimelech, M., 2018. A path to ultraselectivity: support layer properties to maximize performance of biomimetic desalination membranes. Environ. Sci. Technol. 52 (18), 10737–10747.
Xu, P., Duan, S., Li, Z., Hu, M., Zhang, P., Dai, L., Mai, Z., Guan, K., Matsuyama, H., 2024. Charge-sign-independent separation of mono-and divalent ions with nanofiltration membranes. Adv. Funct. Mater., 2416458

Xu, P., Guan, K., Chiao, Y.-H., Mai, Z., Li, Z., Hu, M., Zhang, P., Gonzales, R.R., Matsuyama, H., 2023. Fine-tuning polyamide nanofiltration membrane for ultrahigh separation selectivity of Mg2+ and Li+. J. Membr. Sci. 688, 122133.
Xu, S., Song, J., Bi, Q., Chen, Q., Zhang, W.-M., Qian, Z., Zhang, L., Xu, S., Tang, N., He, T., 2021. Extraction of lithium from Chinese salt-lake brines by membranes: design and practice. J. Membr. Sci. 635, 119441.
Xu, Y., Peng, H., Luo, H., Zhang, Q., Liu, Z., Zhao, Q., 2022. High performance Mg2+/Li + separation membranes modified by a bis-quaternary ammonium salt. Desalination 526, 115519.
Yang, Z., Wang, F., Guo, H., Peng, L.E., Ma, X.-h., Song, X.-x., Wang, Z., Tang, C.Y., 2020. Mechanistic Insights into the role of polydopamine interlayer toward improved separation performance of polyamide nanofiltration membranes. Environ. Sci. Technol. 54 (18), 11611–11621.
Yin, Y., Zhao, Y., Li, C., Wang, R., 2023. Fabrication of polyamide hollow fiber nanofiltration membrane with intensified positive surface charge density via a secondary interfacial polymerization. J. Membr. Sci. 682, 121778.
Yuan, B., Zhang, Y., Qi, P., Yang, D., Hu, P., Zhao, S., Zhang, K., Zhang, X., You, M., Cui, J., Jiang, J., Lou, X., Niu, Q.J., 2024. Self-assembled dendrimer polyamide nanofilms with enhanced effective pore area for ion separation. Nat. Commun. 15 (1), 471.
Yuan, B., Zhao, S., Hu, P., Cui, J., Niu, Q.J., 2020. Asymmetric polyamide nanofilms with highly ordered nanovoids for water purification. Nat. Commun. 11 (1), 6102.
Zhang, L., Hu, M., He, B., Pei, H., Li, X., Matsuyama, H., 2025. A review of the nanofiltration membrane for magnesium and lithium separation from salt-lake brine. Sep. Purif. Technol. 354, 129169.
Zhang, R., Zhu, Y., Zhang, L., Lu, Y., Yang, Z., Zhang, Y., Jin, J., 2021. Polyamide nanofiltration membranes from surfactant-assembly regulated interfacial polymerization: the effect of alkyl chain. Macromol. Chem. Phys. 222 (20), 2100222.
Zhang, S., Wei, X., Cao, X., Peng, M., Wang, M., Jiang, L., Jin, J., 2024. Solar-driven membrane separation for direct lithium extraction from artificial salt-lake brine. Nat. Commun. 15 (1), 238.
Zhao, C., Zhang, Y., Jia, Y., Li, B., Tang, W., Shang, C., Mo, R., Li, P., Liu, S., Zhang, S., 2023. Polyamide membranes with nanoscale ordered structures for fast permeation and highly selective ion-ion separation. Nat. Commun. 14 (1), 1112.
Zhao, Y., Tong, T., Wang, X., Lin, S., Reid, E.M., Chen, Y., 2021. Differentiating solutes with precise nanofiltration for next generation environmental separations: a review. Environ. Sci. Technol. 55 (3), 1359–1376.